

# Compressed Sensing Analog Front-End for Bio-Sensor Applications

Daibashish Gangopadhyay, *Member, IEEE*, Emily G. Allstot, *Student Member, IEEE*, Anna M. R. Dixon, Karthik Natarajan, *Member, IEEE*, Subhanshu Gupta, *Member, IEEE*, and David J. Allstot, *Life Fellow, IEEE*

**Abstract**—In a conventional bio-sensor, key signal features are acquired using Nyquist-rate analog-to-digital conversion without exploiting the typical bio-signal characteristic of sparsity in some domain (e.g., time, frequency, etc.). Compressed sensing (CS) is a signal processing paradigm that exploits this sparsity for commensurate power savings by enabling alias-free sub-Nyquist acquisition. In a severely energy constrained sensor, CS also eliminates the need for digital signal processing (DSP). A fully-integrated low-power CS analog front-end (CS-AFE) is described for an electrocardiogram (ECG) sensor. Switched-capacitor circuits are used to achieve high accuracy and low power. Implemented in 0.13  $\mu\text{m}$  CMOS in  $2 \times 3 \text{ mm}^2$ , the prototype comprises a 384-bit Fibonacci-Galois hybrid linear feedback shift register and 64 digitally-selectable CS channels with a 6-bit C-2C MDAC/integrator and a 10-bit C-2C SAR ADC in each. Clocked at 2 kHz, the total power dissipation is 28 nW and 1.8  $\mu\text{W}$  for one and 64 active channels, respectively. CS-AFE enables compressive sampling of bio-signals that are sparse in an arbitrary domain.

**Index Terms**—Analog-to-digital converters, analog-to-information converters, biomedical sensors, body-area networks, compressed sensing, compressive sampling, ECG, multiplying DAC, SAR ADC, sub-Nyquist sampling, wavelets, wireless sensors.

## I. INTRODUCTION

WEARABLE sensors are increasingly employed in medical monitoring where high energy efficiency, small form factor, multi-signal sensing capabilities and wireless telemetry are essential. A wireless body-area network comprises a heterogeneous set of bio-sensor nodes that communicate with a personal data aggregator such as a smartphone [1].

Key bio-signals have bandwidths of a few kHz, dynamic ranges of  $\sim 40$ – $70$  dB, and structures that are sparse (i.e.,

compressible) in some domain. A conventional bio-sensor (Fig. 1(a)) comprises an analog front-end with signal conditioning and a Nyquist or adaptive-Nyquist analog-to-digital converter (ADC), a DSP block that implements data compression and a radio for short-haul telemetry [2]–[4]. Typically, these functions consume 2%, 25%, and 73%, respectively, of the total power [4].

An alternative architecture (Fig. 1(b)) uses compressed sensing (CS) [5]–[9], an emerging signal processing paradigm, wherein *sparse* input signals digitized by a Nyquist-rate ADC are subsequently compressed using digital-domain CS. CS exploits the low rate of significant events in sparse signals whereas Nyquist sampling processes based on the highest rate of change. Acquisition with CS is independent of the domain of sparsity (time, frequency, etc.), which enables multi-signal sensing capabilities (electrocardiogram (ECG), electroencephalogram (EEG), electromyogram (EMG), etc.).

An analog-domain CS bio-signal acquisition system is shown in Fig. 1(c). The encoder receives a conditioned bio-signal from a low-noise amplifier, and compresses  $N$  input samples,  $[X]$ , into  $M$  output samples,  $[Y]$ , that are digitized and transmitted. The ADC and the RF transmitter operate at sub-Nyquist-rates because the compression factor ( $CF$ ) equals  $N/M$ , which is typically  $\gg 1$ . The receiver (Fig. 1(d)) that resides in the data aggregator down-converts the compressed signal,  $y(t)$ , and uses optimization algorithms to reconstruct a representation,  $\hat{x}(t)$ , of the original signal,  $x(t)$ . In contrast to adaptive-Nyquist sampling [4], CS allows multi-signal sensing capabilities because it is independent of the timing of significant events or the domain of compressibility.

A CS-AFE for bio-sensor applications implemented in 0.13  $\mu\text{m}$  CMOS in  $2 \times 3 \text{ mm}^2$  is described in this paper. It includes 64 channels that are digitally enabled based on the desired  $CF$ . Clocked at 2 kHz, the power dissipation varies from 28 nW for one to 1.8  $\mu\text{W}$  for all 64 active channels. Measurements demonstrate  $CF > 10$  for ECG bio-signals in ambulatory applications.

Section II covers the theory of CS compression and reconstruction, key system requirements and a design methodology. Prior art as well as system design, architecture and circuits of CS-AFE are described in Section III. Measured results are presented in Section IV and conclusions are given in Section V.

## II. CS COMPRESSION AND RECONSTRUCTION

Conventional Nyquist sampling captures the details of a signal whereas CS captures its underlying global structure. For

Manuscript received November 04, 2012; revised September 25, 2013; accepted September 30, 2013. Date of current version January 24, 2014. This paper was approved by Associate Editor Roland Thewes. This work was supported in part by grants from the National Science Foundation (Contract EECs-0951368) and Intel Corporation. The work of A. M. R. Dixon and E. G. Allstot was supported by a Graduate Fellowship and an Undergraduate Research Opportunity Scholarship, respectively, from the Semiconductor Research Corporation.

D. Gangopadhyay is with Marvell Semiconductor, Santa Clara, CA 95054 USA (e-mail: daibash@uw.edu).

E. G. Allstot and A. M. R. Dixon are with the Department of Electrical Engineering, University of Washington, Seattle, WA 98195 USA

K. Natarajan is with Intel Corporation, Hillsboro, OR 97124 USA.

S. Gupta is with Maxlinear, Inc., Irvine, CA 92618 USA.

D. J. Allstot is with the Department of Electrical Engineering and Computer Sciences, University of California, Berkeley, CA 94720-1770 USA.

Color versions of one or more of the figures in this paper are available online at <http://ieeexplore.ieee.org>.

Digital Object Identifier 10.1109/JSSC.2013.2284673

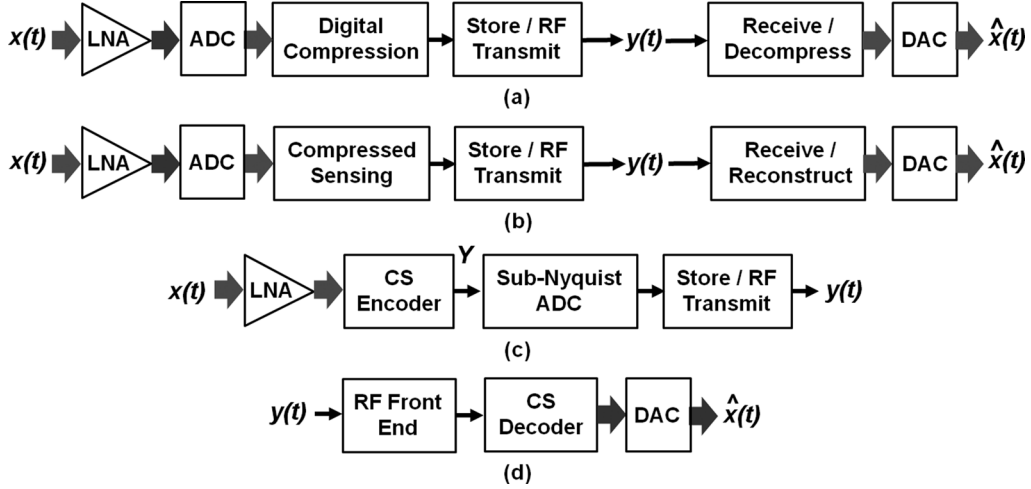


Fig. 1. Bio-signal acquisition. (a) Nyquist ADC followed by digital compression; (b) Nyquist ADC followed by digital-domain compressed sensing, (c) an analog-domain CS transmitter and (d) a CS receiver.

a sparse signal with  $S$  tones, for example, conventional Nyquist processing requires sampling faster than twice the highest frequency regardless of  $S$ , which results in large number of samples. DSP-based transform coding (e.g., Discrete Fourier Transform) is then used to extract the  $S$  Fourier coefficients. Even though it performs time-domain sampling, CS exploits the frequency-domain sparsity so that only about  $2S$  samples (acquired directly) are needed for exact recovery at the receiver. Thus, CS compresses without the power and area needs of a basis transformation (FFT, DCT, etc.) hardware. Knowledge of the basis of sparsity is needed only in the receiver which is usually less energy constrained than the sensor.

### A. Compressed Sensing

Compression with CS is defined by the simple matrix equation  $[Y] = [\Phi][X]$  wherein an uncompressed *input vector*  $[X]$  of size  $N$  multiplied by a *measurement matrix*  $[\Phi]$  of size  $M \times N$  produces a *measurement vector*  $[Y]$  of size  $M < N$  (Fig. 2(a)) [5]–[7]. Because  $[\Phi]$  is an array of random numbers (e.g., Bernoulli, Gaussian, uniform, etc.),  $[Y]$  is a vector of *random linear projections* of  $[X]$  on  $[\Phi]$ . CS can compress bio-signals by  $CF > 10$ , which reduces the data to be transmitted and, thus, the total power dissipation in the sensor node by a similar factor.

Sparsity is quantified herein as  $(1 - K/N)$  where  $K$  is the number of significant values among the  $N$  input samples.  $[X_K]$  is derived from  $[X]$  by zeroing the insignificant coefficients. Sparsity means  $[X_K] \sim [X]$ ; i.e., the  $l_2$ -norm of the residue,  $\|X - X_K\|_2$ , is small. The minimum number of measurements needed for accurate reconstruction is  $M \geq p \log(N/K) > 2K$  where  $p$  is a constant [8].

### B. CS Reconstruction

Generally, reconstruction in the receiver is more time and power consuming than compression in the transmitter. However, this is well-suited for applications where the data aggregator (receiver) has much greater computational and energy resources than the sensor. For a signal sparse in an arbitrary domain,  $[X] = [\Psi][\alpha]$ , where  $[\Psi]$  is an  $N \times N$  *sparsifying basis*

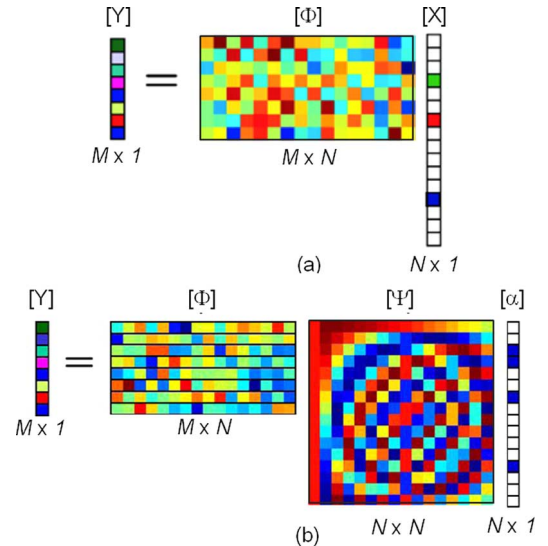


Fig. 2. CS formulations for a generic CS (a) encoder and (b) decoder. The shaded squares in  $[\Phi]$  and  $[\Psi]$  represent the different amplitudes of the random coefficients; the white boxes in  $[X]$  and  $[\alpha]$  represent insignificant or zero signal values.

and  $[\alpha]$  is the corresponding sparse representation of  $[X]$  in the basis  $[\Psi]$  (Fig. 2(b)). For example, if  $x(t)$  is sparse in the time (frequency) domain,  $[\Psi]$  is an Identity (Inverse Fourier Transform) matrix. Two conditions ensure accurate reconstruction:  $[X]$  is sparse in  $[\Psi]$ , and  $[\Psi]$  and  $[\Phi]$  are *incoherent* [5], [8].

Ideally,  $[\hat{X}] = [\Phi]^{-1}[Y]$ , where  $[\hat{X}]$  is the reconstructed vector. However, as  $[\hat{X}]$  has  $N$  unknowns and  $[Y]$  has only  $M$  knowns,  $[\Phi]$  is non-square and non-invertible. Thus, optimization algorithms are needed for reconstruction. The  $l_1$ -norm is an accurate measure of the sparsity of  $[\alpha]$ , which is recovered using optimization of the objective function [5], [6]:  $\text{Min } \|\alpha\|_1$  subject to  $[Y] = [\Phi][\Psi][\alpha]$ . The reconstructed signal is  $[\hat{X}] = [\Psi][\alpha]$ . For time-domain sparse signals where  $[\Psi] = [I]$ ,  $[\hat{X}]$  can be recovered in one step:  $\text{Min } \|\hat{X}\|_1$  subject to  $[Y] = [\Phi][\hat{X}]$ .

The process of finding the minimum  $l_1$ -norm solution is called *basis pursuit* (BP). Various BP algorithms trade off

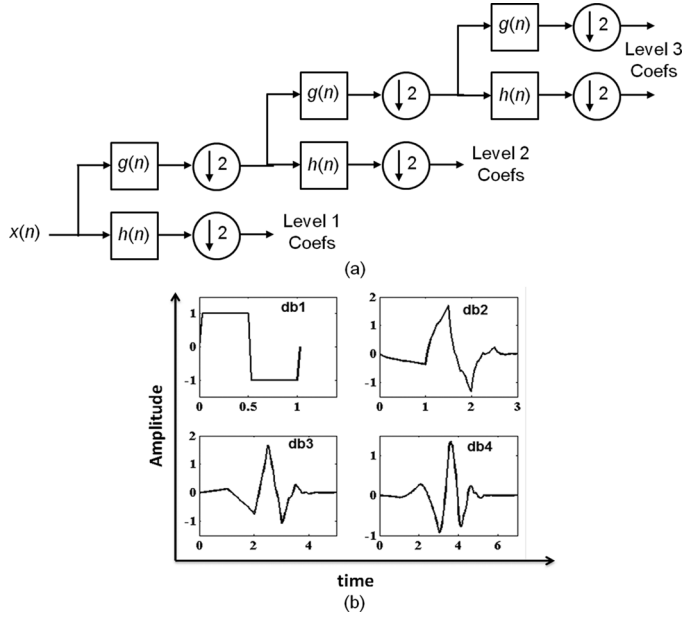


Fig. 3. (a) Three-level tree structure for decomposed wavelet coefficients and (b) several example Daubechies mother wavelets [31].

computation time versus accuracy for various signal structures [9]–[12]. Accuracy is defined using an  $l_2$ -norm-based signal-to-error ratio (SER):

$$\text{SER} = 20 \log_{10} \left( \frac{\|X\|_2}{\|X - \hat{X}\|_2} \right). \quad (1)$$

A comparison of reconstruction algorithms is presented in [13].

### C. The Sparsifying Matrix

$[\Psi]$  is an  $N \times N$  identity matrix for time-domain-sparse bio-signals. For bio-signals sparse in frequency domain, reconstruction requires that  $[\Psi]$  be an inverse Fourier transform matrix, or an inverse Gabor transform matrix, etc. The wavelet domain, widely used for ECG signals with  $[\Psi]$  as an inverse wavelet transform matrix, uses multi-scale decompositions. Wavelet coefficients are typically generated hierarchically using scale-dependent low-pass ( $h(n)$ ) and high-pass ( $g(n)$ ) quadrature mirror filters that correspond to the type of wavelet (i.e., the mother wavelet) (Fig. 3(a)) [14]. The choice of mother wavelet plays a key role in signal recovery. For example, ECG signals are often reconstructed using Daubechies wavelets (Fig. 3(b)) because their scaling and time dilations approximate typical ECG pulses (i.e., QRS complexes). The result is a sparse representation in the wavelet basis [11], [12].

### D. Sparsity, Restricted Isometry and Incoherence

1) *Sparsity*: The domain of sparsity is apparent for signals such as  $K$ -tone sinusoids that are sparse in the Fourier domain. Because many signals are sparse in multiple domains, the feature of interest determines the domain for reconstruction. For example, for applications where only heart rate information is desired, an ECG signal can be thresholded to increase its sparsity and processed in the time domain [13], [15], [16]. For appli-

cations where more signal features are required, un-thresholded ECG waveforms are often reconstructed in the wavelet domain [17], [18].

It is useful to calculate the sparsity of a conditioned ECG signal. For 8-bits of resolution and  $V_{FS} = 1.024$  V, the digitized signal is effectively thresholded at the 1 LSB level; i.e., values  $< 4$  mV are resolved as zero. Simulations on several frames of PhysioBank® data [19] with  $N = 1024$  show that on average  $K \sim 68$  wavelet coefficients are significant with  $\sim 16$  connected-tree components that introduce redundancy [12], [14]. Thus, with an effective  $K \sim 68 - 16 = 52$ , the signal is  $\sim 95\%$  sparse and  $\sim 6X$  compressible [13].

2) *Restricted Isometry Property and Incoherence*: Accurate reconstruction is possible only when  $[\Phi]$  satisfies the Restricted Isometry Property (RIP) [8].  $[\Phi]$  has an RIP of order  $K$  if

$$(1 - \delta_K) \leq \frac{\|[\Phi][X]\|_2^2}{\|X\|_2^2} \leq (1 + \delta_K) \quad (2)$$

where  $\delta_K$  is the isometry constant. RIP does not hold for  $K > M$ . Satisfying RIP implies that no two  $x$  values map to the same  $y$  value, which enables robust reconstruction. RIP is satisfied by many random measurement matrices including Bernoulli, Gaussian, etc.

Because RIP is useful but difficult to validate directly [8], it is often replaced by an equivalent requirement that  $[\Phi]$  and  $[\Psi]$  exhibit a small coherence,

$$\mu(\Phi, \Psi) = \sqrt{N} \max_{1 \leq k, j \leq N} |\langle \phi_k, \psi_j \rangle| \quad (3)$$

where  $1 < \mu(\Phi, \Psi) < \sqrt{N}$  is the range of coherence values between any row of  $[\Phi]$  and any column of  $[\Psi]$ . The greater the coherence the greater the number of measurements needed for accurate reconstruction and the lower the compression factor. Independent and identically distributed (i.i.d.) random matrices provide low coherence values ( $\sim (2 \log_2 N)^{1/2}$ ) with any fixed  $[\Psi]$  for a variety of sparsifying bases [6], [8].

### E. System Modeling

An approach for the design of a complete CS system is as follows:

- 1) Identify a suitable basis  $[\Psi]$  in which the signal has a compact representation in order to minimize the number of significant coefficients ( $K$ ) in  $[\alpha]$ .
- 2) Choose an i.i.d. random number distribution for  $[\Phi]$  to minimize  $\mu(\Phi, \Psi)$ .
- 3) Apply CS using  $[Y] = [\Phi][X]$  and transmit. At the receiver minimize the  $l_1$ -norm of  $[\alpha]$ , solve  $[Y] = [\Phi][\Psi][\alpha]$  using a greedy or global optimization algorithm and recover the signal using  $[\hat{X}] = [\Psi][\alpha]$ .
- 4) Tune the objective function of the optimization algorithm (e.g., relax the error bounds for signals corrupted by noise and artifacts), and evaluate the accuracy using sample data sets.
- 5) Implement the ability to dynamically trade off the compression factor versus accuracy to maximize energy efficiency.

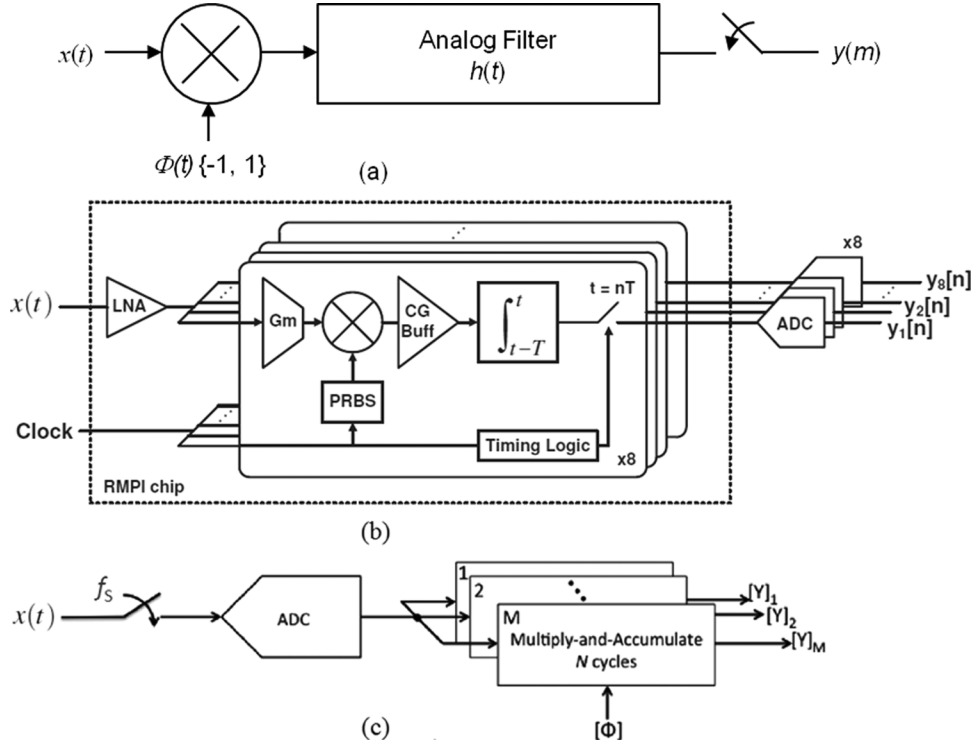


Fig. 4. Prior art compressed sensing architectures. (a) Random demodulator [20], (b) random modulation pre-integrator [21], and (c) a digital-domain CS based data compressor [24], [25].

### III. ARCHITECTURE AND CIRCUIT DESIGN

#### A. Prior Art

Kirolos *et al.* [20] developed an analog-to-information converter—the random demodulator (RD)—for processing sparse multi-tone signals (Fig. 4(a)). The compressed signal is generated by multiplying the analog input signal by a chipping sequence (e.g., at  $>4X$  the Nyquist-rate) using a Gilbert mixer and integrating using an active RC integrator. Simulations show that a three-tone AM signal is recovered accurately using an ADC operated at  $1/6$  the Nyquist-rate. Ragheb *et al.* [21] implemented RD using discrete components and a commercial DSP board for reconstruction. Output SNR values (not SER as defined in (1)) of 45.5, 42.9, and 39.6 dB were obtained with the ADC operated at  $1/2$ ,  $1/4$ , and  $1/8$  the Nyquist-rate, respectively. Mishali *et al.* [22] described a modulated wideband converter (MWC) wherein the input signal is processed using a parallel set of sub-Nyquist chipping sequences; i.e., MWC is a variant of RD that enables sub-Nyquist sampling of multi-band frequency-sparse signals. Yoo *et al.* [23] presented a CS sub-Nyquist RF receiver that uses the random modulator pre-integrator (RMPI) architecture of Fig. 4(b) to compress radar pulse signals. The chip integrates an RF low-noise amplifier (RF-LNA) and eight RMPI channels, compressed senses RF pulses which have 0.1–2 GHz bandwidth and consumes 506.4 mW, excluding the off-chip A/D converters. Chen *et al.* [24], [25] introduced a digital-domain implementation of CS (Fig. 4(c)) for bio-sensor applications. Nyquist-rate A/D conversion is followed by digital multiply and accumulate (MAC) operations. The 8-bit Nyquist-rate SAR ADC occupies  $90 \times 150 \mu\text{m}^2$  and the 50 16-bit MAC blocks occupy  $200 \times 450 \mu\text{m}^2$  in 90 nm CMOS. Clocked at 1 kHz, the

power dissipation of the chip is  $1.9 \mu\text{W}$  from  $V_{DD} = 0.6 \text{ V}$  and  $\sim 20 \mu\text{W}$  from  $V_{DD} = 1 \text{ V}$  (due to leakage currents).

In this paper a universal CS-AFE architecture (Fig. 5) for compressing bio-signals that are sparse in any domain is described, obviating DSP hardware. Here analog-domain CS scheme is implemented using switched-capacitor (SC) techniques which enable alias-free sub-Nyquist A/D conversion and significant energy savings.

#### B. CS-AFE Architecture

A column-by-column matrix multiplication is used to compute  $[Y] = [\Phi][X]$  in the CS-AFE as it enables pipelined operation and a continuously-sampled input signal. For example, the first input sample,  $x(t = T_s) = X_1$ , multiplied by the first column of  $[\Phi]$  produces  $M$  partial products,  $\{\Phi_{11}X_1, \Phi_{21}X_1, \dots, \Phi_{M1}X_1\}$ , the second input sample,  $x(t = 2T_s) = X_2$ , multiplied by the second column of  $[\Phi]$  generates another  $M$  partial products,  $\{\Phi_{12}X_2, \Phi_{22}X_2, \dots, \Phi_{M2}X_2\}$ , and so on. In each of the  $M$  channels, the corresponding partial sums are added over a frame of  $N$  cycles. Thus, at the end of the frame when  $t = NT_s$ ,  $y_1(t = NT_s) = Y_1 = \Phi_{11}X_1 + \Phi_{12}X_2 + \dots + \Phi_{1N}X_N$ ,  $y_2(t = NT_s) = Y_2 = \Phi_{21}X_1 + \Phi_{22}X_2 + \dots + \Phi_{2N}X_N, \dots$ , and  $y_M(t = NT_s) = Y_M = \Phi_{M1}X_1 + \Phi_{M2}X_2 + \dots + \Phi_{MN}X_N$ . The resulting compressed vector,  $[Y]$ , is identical to the random linear projections generated by conventional row-column matrix multiplications.

Each compressed value,  $Y_i$ , is computed using an SC multiplying digital-to-analog converter/integrator (MDAC/I), and a sub-Nyquist SC SAR ADC. Each MDAC/I samples at  $f_s = \text{Nyquist-rate}$  ( $f_{\text{NYQ}}$ ) and each ADC operates at a sub-Nyquist

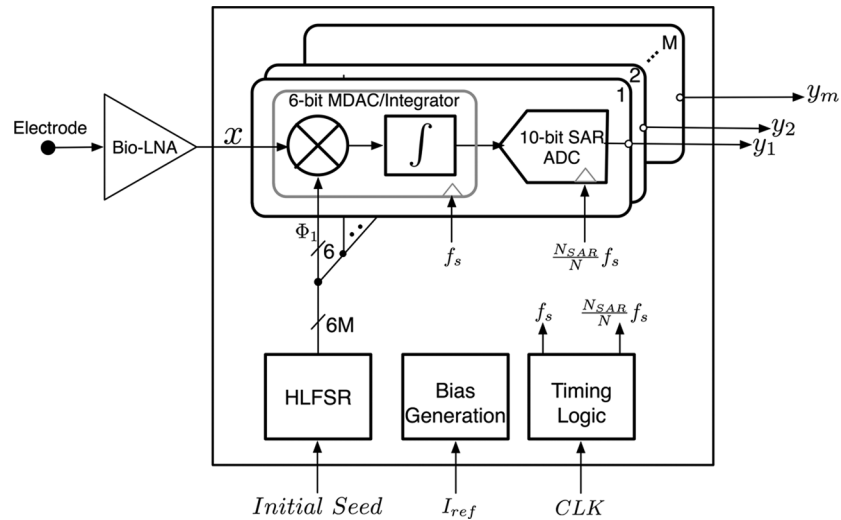


Fig. 5. Architecture of CS-AFE.

rate  $(N_{\text{SAR}}/N f_s)$ ,  $N \gg N_{\text{SAR}}$ , where  $N_{\text{SAR}}$  is the number of clock cycles needed to reset, sample and encode each sample. The decoupling of the sampling rates saves power without introducing any aliasing. Key attributes of the CS-AFE architecture include:

- Pipelined operation;
- Multiplication at the Nyquist-rate and digitization at a sub-Nyquist-rate;
- Energy-efficient low-frequency SC circuits scalable to different sampling rates;
- Hardware complexity of  $O(M)$ ;
- A digitally-programmable number of MDAC/I integration cycles,  $N$ , per frame;
- Accurate multiplication, integration and digitization limited only by capacitor mismatch.

### C. CS-AFE System Design Considerations and Specifications

The design specifications for CS-AFE are different from a traditional AFE because CS is inherently lossy; i.e., CS achieves similar accuracy as Nyquist-rate A/D conversion followed by lossy digital compression. Several non-idealities limit the accuracy of CS:

#### 1) Reconstruction Accuracy, Signal Sparsity and Signal Features

- a) The reconstruction process in a Nyquist-rate acquisition system is ideally linear and does not limit SER. By contrast, SER in a CS system is limited by the finite error bounds of the reconstruction algorithm; variants of greedy or global optimization algorithms are typically used with  $l_1$ -norm as the sparsity metric [13].
- b) Signal sparsity affects reconstruction accuracy—with less sparsity the reconstruction error is greater even for an algorithm with low error bounds. The error bounds are usually determined for highly sparse signals. For signals of moderate sparsity, however, the non-linear and probabilistic characteristics of the recovery algorithms make exact SER and

resolution predictions problematic. Moreover, the sparsity changes dramatically between frames for some bio-signals; e.g., EEG, EMG, etc. As a consequence, the SER of a reconstructed highly-sparse tone signal is substantially higher than that of a moderately-sparse bio-signal.

- c) Time-domain thresholding (i.e., zeroing) of signal details below a pre-defined level can be used to control sparsity [13]. Thus, the increased accuracy of the reconstruction process is traded off against the reduced SER of the signal due to the initial thresholding.

#### 2) Noise and Non-linearity

- a) A signal can be treated as the sum of the ideal signal and noise components because the signal and noise are uncorrelated. When CS operates on the sum, the signal vector is incoherent with the measurement matrix and reconstructed as expected. Ideally, the noise vector is coherent with the random measurement matrix and not reconstructed. This benefit is also understood from the accumulation action of the MDAC/I circuit. It multiplies the noise vector by a random matrix and integrates, which is equivalent to noise averaging over  $N$  cycles. Thus, there is an effective de-noising for AWGN noise. However, colored noise can be incoherent with the measurement matrix and decreases sparsity.
- b) Non-linearities in the Bio-LNA increase the in-band harmonics and spurious features in  $[X]$ , which reduces sparsity. These signal components are reconstructed accurately because they are also incoherent with the measurement matrix; hence, the maximum SER and achievable compression factor are reduced. The MDAC/I and ADC circuit non-linearities distort the compressed signal,  $[Y]$ , which also reduces the accuracy of reconstruction.

In many cases (e.g., some ECG ambulatory applications) accurate time-domain reconstruction of the entire signal is not required. Instead, global features are found. In [24], for example,

although the reconstructed EEG and ECG signals have SNR values of only 1–10 dB, the EEG spike timing and the ECG R-R intervals (i.e., heart rates) are accurately extracted. From a system design point of view, the effects of MDAC/I thermal noise, ADC quantization noise and non-linearity can be decoupled as they have different impacts on the non-linear CS reconstruction algorithms.

### 3) Gain and Noise Specification

The gain and noise specifications for ambulatory bio-signal sensors typically require up to 8 bits of resolution. At the sensor electrode, the raw bio-signals have dynamic ranges  $> 40$  dB (excluding DC level variations, spurious tones, etc.), with different signals having different peak amplitudes; e.g., ECG signal peaks are  $10 \text{ mV}_{pp}$  differential. Thus, for  $\sim 8$ -bit resolution of ECG signals, the input-referred noise should be less than  $14.7 \mu\text{V}_{rms}$ . State-of-the-art Bio-LNAs achieve an input-referred noise of  $< 2 \mu\text{V}_{rms}$  over a 1 kHz bandwidth using chopper-stabilized circuits [4]. The remaining noise power is budgeted for input-referred noise contributions from the MDAC/I circuits for the worst-case condition when all  $M$  rows are active. A nominal Bio-LNA gain of 80 V/V is needed to amplify the  $< 10 \text{ mV}_{pp}$  ECG signals to the  $800 \text{ mV}_{pp}$  differential full-scale range of the MDAC/I circuits. Gain programmability over a 20–40 dB range and a sub-Hz high-pass filter are also needed to accommodate sensor electrode impedance variations and dc offset voltages, respectively.

The total noise power from the Bio-LNA and  $M$  active MDAC/I circuits referred to sensor electrode is  $\sigma_n^2 = (2 \mu\text{V})^2 + (M kT/C_{in})/80^2 = (14.7 \mu\text{V})^2$ , where  $k$  is the Boltzmann constant. This sets  $C_{in}$  for the MDAC/I circuit at  $\sim 200 \text{ fF}$ , for  $M = 64$ . In cases where  $M < 64$  rows are active (i.e., higher  $CF$ ), the input-referred noise is lower. Note that for different bio-signals (e.g., ECG, PPG, etc.), the peak signal levels are different; hence, the gain should be programmable to utilize the full-scale range of the MDAC/I circuits to maintain a similar SNR.

### 4) Non-linearity and ADC Specification

Non-linearities in the Bio-LNA decrease the sparsity of the signal in  $[X]$  and thus reduce the accuracy of reconstruction. For simplicity we assume a third order non-linear model for MDAC/I and ADC. For HD3 to degrade the SNDR of the Bio-LNA by  $< 0.5 \text{ dB}$ , it should be  $> 9 \text{ dB}$  less than maximum SNR for 8-bit resolution, i.e.,  $\text{HD3} < -58 \text{ dBc}$ . When the measurement matrix is composed of Bernoulli random numbers, each MDAC/I operates as a 1-bit coefficient multiplier and integrator. As a consequence, MDAC/I gain non-linearity depends on the matching accuracy between the integration and sampling capacitors (e.g.,  $\sim 10.5$  bits for 200 fF capacitors). The non-linearity (HD3) and finite settling errors of the ADC cause non-linearities in the compressed signal  $[Y]$  but not on the input signal directly. The effect of these non-linearities along with ADC quantization noise were studied empirically for Fourier-domain sparse signals. Fig. 6 shows the reconstructed SER versus ADC resolution for different HD3 for a one-tone signal with  $N = 256$  samples and  $CF = 2, 4,$  and  $8$  averaged over 300 trials. Here the non-linear reconstruction process is seen to limit the maximum reconstruction SER to about 32 dB even for highly-sparse signals conditioned by a highly-linear

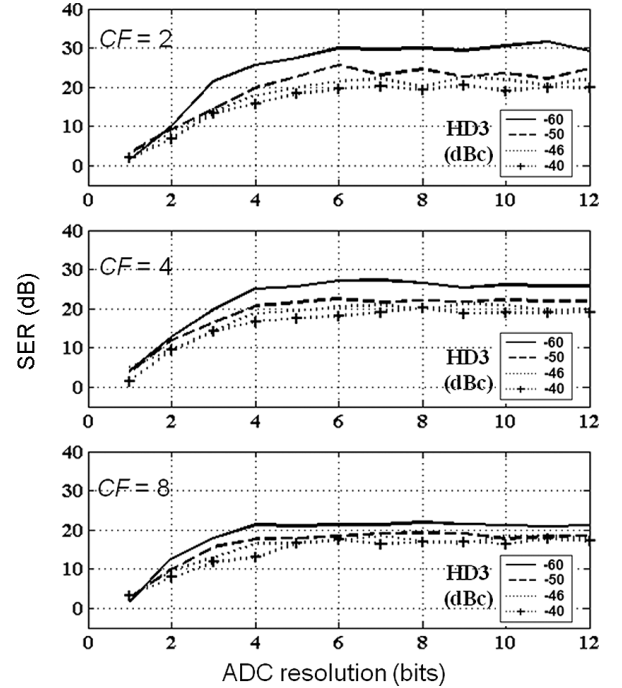


Fig. 6. Reconstruction SER vs. ADC resolution and HD3 for a single-tone signal.  $N = 256$  and  $[\Psi] =$  Inverse Fourier Basis.

front end. This limitation is due to the error bounds of the reconstruction algorithm, the short time window of the tone signal which decreases the Fourier-domain sparsity, and the non-ideal incoherence of the measurement and sparsifying matrices. On average, the reconstruction SER does not improve by more than 4 dB as the ADC resolution is increased from 6 to 12 bits. Also, improving HD3 below  $-50 \text{ dBc}$  does not increase reconstruction SER consistently by more than 3 dB for  $CF > 4$ . ADC resolutions of 6–10 bits show similar reconstruction SER. Thus, an 8-bit ENOB performance was targeted with  $\text{HD3} < -50 \text{ dBc}$ . Because ADC ENOB is typically 1–2 bits less than the resolution when calibration is not used, a 10-bit C-2C capacitor DAC is used. For  $CF > 4$ , both requirements can be relaxed to reduce die area and power consumption.

To the first order, the input DC offset voltage of the MDAC does not affect the integration. However, switch charge-injection errors can accumulate depending on the random switching sequence and the number of integration cycles,  $N$ . The accumulated offset voltage is sampled by the ADC and calibrated out.

$M$  and  $N$  are chosen based on area constraints and system simulations. The layout height of each row is determined by MDAC/I and ADC capacitance dimensions noting that square capacitor layouts exhibit the best matching. With each row  $\sim 36 \mu\text{m}$  tall, a maximum of 65 rows (including test structures) can be integrated in 2.5 mm. Thus,  $M = 64$  was used for this design. To enable a minimum  $CF = 2$ , a minimum  $N = 128$  was chosen. Both  $M$  and  $N$  are programmable ( $M = [1-64]$ ,  $N = [128, 256, 512, 1024]$ ) to achieve  $CF = 2-1024$ .

The specifications for CS-AFE are summarized in Table I.

### D. Timing and Synchronization

The overall timing for CS-AFE is shown in Fig. 7. For each of the  $M$  channels  $N$  input samples are processed at the Nyquist-

TABLE I  
SYSTEM SPECIFICATIONS FOR THE CS-AFE

Parameter	Bio-LNA					MDAC/I	SAR ADC
Gain Range (dB)	20 - 60 (38 nominal)					-15.6 - 0	0
Full Scale (V)	10 mV <sub>p-p</sub> (Differential)					0.8 V <sub>p-p</sub> (Differential)	0.8 V <sub>p-p</sub> (Single-ended)
Sensor-referred Noise ( $\mu\text{V}_{\text{RMS}}$ )	< 2					< 14.5/ $\sqrt{M}$	< 0.1
HD3 (dBc)	< - 60					< - 50	< - 50
Bandwidth (BW) (Hz)	ECG <sup>1</sup>	PPG <sup>2</sup>	EMG <sup>3</sup>	ECoG <sup>4</sup>	EEG <sup>5</sup>		
Ambulatory (< 8 bits)	40	20	200	200	100	> 5 X BW Bio-LNA	1/N X BW Bio-LNA
Diagnostic (< 12 bits)	150	50	600	6 k	10 k	> 9 X BW Bio-LNA	[N = 128, 256, 512, 1024]

<sup>1</sup>ECG – Electrocardiogram (monitors cardiac rhythm)

<sup>2</sup>PPG – Photoplethysmogram (monitors arterial oxygen saturation level)

<sup>3</sup>EMG – Electromyogram (monitors muscular movements and anomalies)

<sup>4</sup>ECoG – Electrocochogram (monitors brain activity by probing the cortex)

<sup>5</sup>EEG – Electroencephalogram (monitors brain activity by probing the scalp; alpha, beta and gamma waves limited to 100 Hz, while spikes typically limited to 10 kHz).

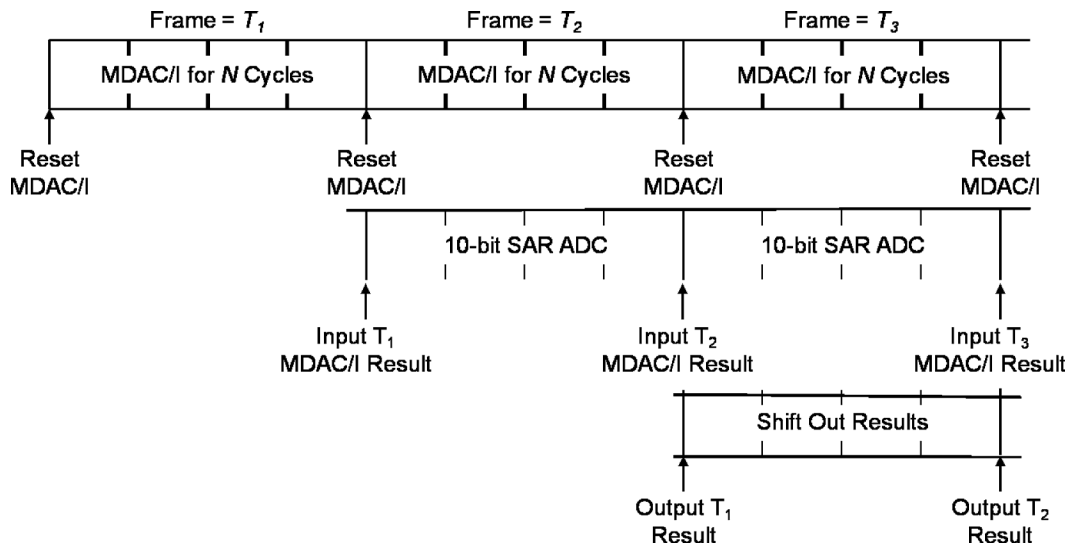


Fig. 7. Pipelined operation of the CS-AFE. The MDAC/I circuit is reset at the beginning of a frame (e.g.,  $T_1$ ) of  $N$  samples (e.g.,  $N = 256$ ). Its output is sampled at the end of  $T_1$  and the SAR ADC converts during  $T_2$ . The results are multiplexed out in a bit-parallel fashion and post-processed in *MATLAB*®.

rate over the frame time,  $T_1$ . The corresponding SAR A/D conversion is pipelined during the next frame,  $T_2$ . The DC offset voltage of each MDAC/I is cancelled at the beginning of each frame. The ADC conversion rate is  $1/N$  of the Nyquist-rate; i.e., the SAR ADC clock runs at  $N_{\text{SAR}}/N$  of the Nyquist-rate.

#### E. On-Chip Generation of the Random Measurement Matrix

At least 6-bit coefficients are needed for accurate reconstruction using Gaussian or uniform random  $[\Phi]$  matrices [15] whereas 1-bit coefficients are adequate for Bernoulli, Toeplitz, etc., implementations [13], [26]. CS-AFE generates both Bernoulli and uniform random measurement matrices for operation with different input bio-signals and sparsifying bases.

For a 6-bit uniform distribution,  $6MN$  total bits are needed in  $[\Phi]$ . If stored on-chip,  $N = 256$  and  $M = 64$  for example, would require 98,304 SRAM bits, which consumes significant area and power when operated at the Nyquist frequency; these drawbacks worsen with increased  $N$ .

CS-AFE employs an on-chip hybrid linear feedback shift register (HLFSR) (Fig. 8) to synthesize  $[\Phi]$ : First, a 6-bit *Fibonacci* LFSR cell is constructed for use with each 6-bit coefficient of  $[\Phi]$ . Next, the seed for each 6-bit LFSR is further randomized by dithering its LSB input in a *Galois* fashion. Eight such stages are cascaded to form the 48-bit *Fibonacci-Galois* HLFSR block shown. Finally, eight of these 48-bit blocks are cascaded to generate 64 rows of 6-bit random coefficients. The 1-bit Bernoulli  $[\Phi]$  matrix is formed using only the MSBs of the 6-bit LFSRs;



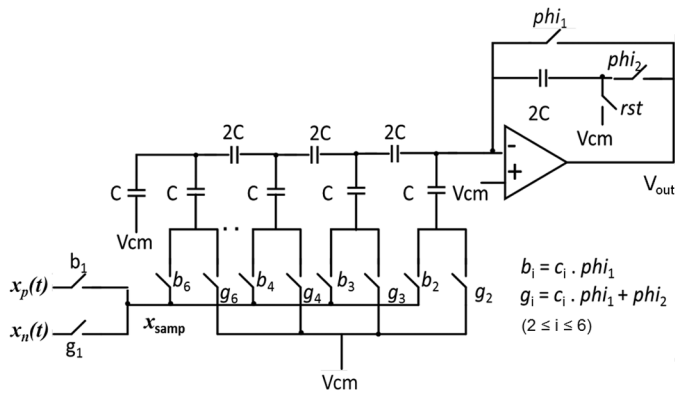


Fig. 9. A six-bit switched-capacitor C-2C MDAC/I where  $c_i$  is the  $i^{\text{th}}$  bit of a 6-bit random coefficient generated by the HLFSR. Bits  $c_2 - c_6$  are set to 1 for one-bit random (e.g., Bernoulli) coefficients.

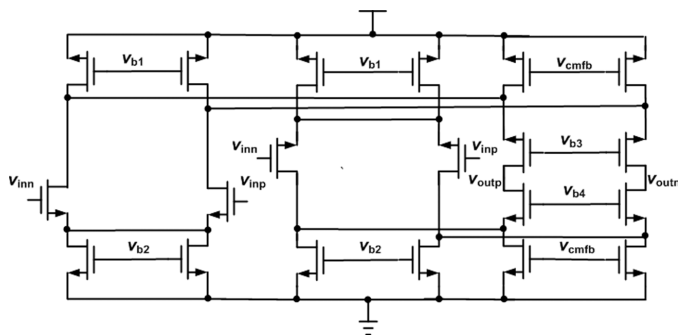


Fig. 10. The fully-differential sub-threshold folded-cascode operational amplifier.

reliably without calibration techniques. Thus, the CS-AFE uses a C-2C DAC array (Fig. 9) where the total input capacitance is only  $2C_u$  ( $\sim 200$  fF), i.e., a unit capacitance  $C_u = 100$  fF, which meets the matching requirements without any calibration. For a Bernoulli measurement matrix only the MSB (sign bit) of HLFSR is used; the other bits are set to one. Thus, the input capacitance is identical for the  $+1/-1$  coefficients, which eliminates MDAC/I gain errors.

For low-noise, low-power and moderate closed-loop BW, a sub-threshold biased op amp is an optimal choice because it provides high current efficiency at kHz bandwidths. The sub-threshold folded-cascode op amp of Fig. 10 realizes an open-loop gain of  $\sim 36$  dB and a unity-gain bandwidth of  $> 5$  kHz, which provides adequate closed-loop gain and small-signal settling accuracies for the C-2C SAR ADC. A typical  $g_m/I_D > 20 \text{ V}^{-1}$  is achieved using a bias current of 10 nA. The MDAC/I circuit is designed for a nominal closed-loop gain of  $\sim 1/3$  to prevent saturation at the output during integration.

### G. SC C-2C SAR ADC

The thermal noise limit for the SAR ADC dictates  $(kT/C_{in})^{1/2} < 1/2V_{FS}/2^{\text{ENOB}}$ . For a full-scale voltage of 800 mV<sub>pp</sub> and an 8-bit ENOB,  $(kT/C_{in})^{1/2} < 1/2(0.8/2^8) \Rightarrow C_{in} = 1.7$  fF, a tiny input capacitance. However, capacitor matching dominates the choice of unit capacitance ( $C_u$ ) and, hence, the input capacitance. A conventional SAR ADC uses a binary-weighted capacitor array [27], which consumes large

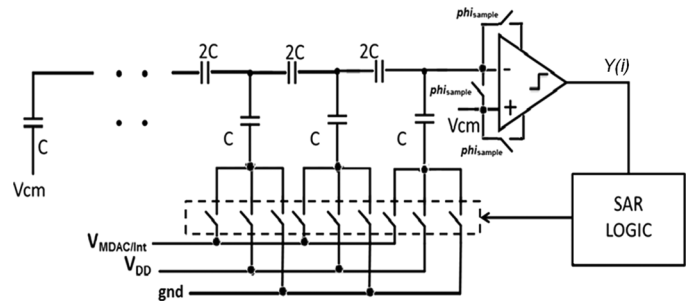


Fig. 11. The C-2C SAR ADC. Dual-gate switches and logic gates are used to minimize leakage currents.

area and requires a total array capacitance of  $2^n C_u$ . Since this approach also requires a separate sampling buffer, a C-2C SAR ADC (Fig. 11) [28] is used instead wherein the input sampling capacitance is reduced from  $2^n C_u$  to  $2C_u$  and the total capacitance is only  $3nC_u$ . Thus, the C-2C architecture minimizes dynamic power dissipation and eliminates the input sampling buffer. Careful layout is needed to ensure that routing and switch parasitic capacitances do not adversely affect capacitor matching. Based on simulations, a unit capacitance of 200 fF was chosen to meet the matching requirements and to implement the MDAC/I closed-loop gain of  $1/3$ . The performance of the C-2C ADC is limited by capacitor parasitics and sampling switch non-linearities. To achieve an 8-bit ENOB, a 10-bit C-2C capacitor DAC is implemented to reduce quantization noise and budget for static gain non-linearity.

### H. Sub-Threshold Pre-Amplifier and Latch

The comparator comprises two pre-amplifier stages and a differential latch (Fig. 12). The signal from MDAC/I is sampled onto the capacitor array with the pre-amps in unity-gain to also store the input-referred DC offset voltage. The gain of the two-stage pre-amp is high (e.g., 40 dB) to limit the preamp input-referred DC offset voltage to within  $1/2$  LSB or 0.4 mV for an estimated worst-case latch input offset voltage of 40 mV. A fully-differential pre-amp topology is used to reduce kick-back voltage errors from the latch to the comparator input. The pre-amp uses positive-feedback for increased gain [29]. The overall pre-amplifier circuit comprises two identical stages. Relatively large input devices ( $120 \mu\text{m}/1 \mu\text{m}$ ) are used to reduce  $1/f$  noise. The total gain of 38 dB and overall unity gain bandwidth of 120 kHz is achieved from the two-stage pre-amp with a bias current of 15 nA. With a 20%  $g_m$  PVT variation, the gain of the pre-amp varies from 36–39 dB. In the worst case, the input offset voltage is  $40 \text{ mV}/10^{(36/20)} = 0.64$  mV which is  $< 1$  LSB.

The key aspects of the latch design are:

- (i) *Leakage current during reset:* The latch operates in the sub-threshold region. In combination with the SAR ADC, it is reset during the first phase of each bit-cycle. At sub-kHz frequencies, leakage power dissipation during the reset time can be significant. The design of Fig. 12 limits the leakage current to pA levels using transistor stacking to increase the effective channel length. Because gate leakage currents in a 130 nm CMOS process can

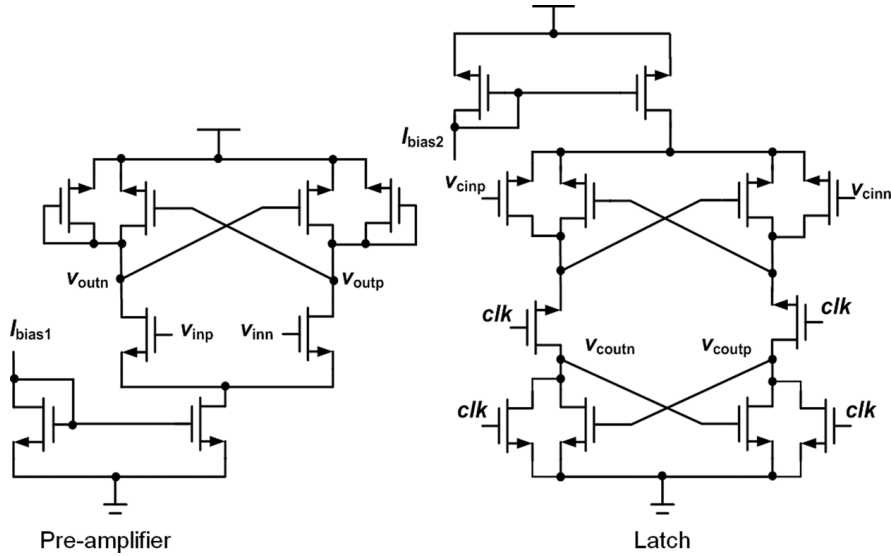


Fig. 12. The pre-amplifier and latch circuits of the comparator.

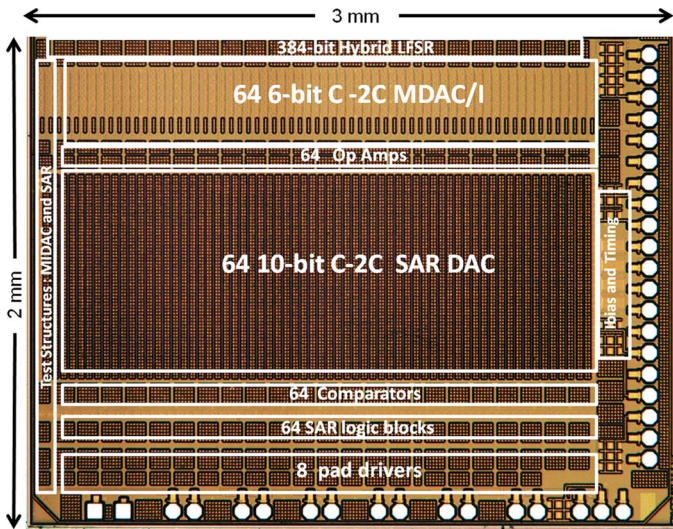


Fig. 13. Die photo of the  $0.13 \mu\text{m}$  CMOS  $2 \times 3 \text{ mm}^2$  CS-AFE.

also be problematic, all sampling switches and digital logic gates use thick-oxide dual-gate devices.

- (ii) *Common-mode level*: In sub-threshold operation, the output common-mode voltage of the NMOS pre-amplifier stage is typically  $> V_{DD}/2$  for an input common-mode voltage of  $V_{DD}/2$ . DC level shifters are avoided using a PMOS input stage for the latch.

#### IV. EXPERIMENTAL RESULTS

CS-AFE was fabricated in  $2 \times 3 \text{ mm}^2$  in a  $0.13 \mu\text{m}$  IBM RF CMOS process (Fig. 13). It allows parallel loading an initial seed sequence into the HLFSR for testing with various bio-signals using 1-bit Bernoulli or 6-bit uniform random coefficients. The frame time is programmable over  $N = 128, 256, 512$ , and 1024 Nyquist sampling cycles and the number of CS channels,

$M$ , is selectable from 1–64; hence,  $CF$  is programmable from 2 to 1024. Extra cells are included to test the MDAC/I and SAR ADC circuits separately. All timing and sampling clocks are derived from an external clock. The clock and input signal are generated by arbitrary waveform generators. The digital words output from the 64 ADC stages are multiplexed to output pad drivers connected to a logic analyzer. The results are post-processed using MATLAB®.

Shown in Fig. 13, each channel of CS-AFE has a height of  $\sim 36 \mu\text{m}$ . The 6-bit HLFSR, 6-bit MDAC/I and the 10-bit SAR ADC are laid out with careful consideration to capacitor matching in the C-2C sections. CS-AFE is packaged in a low-cost-80-lead LQFP80A plastic package with package parasitics being negligible at kHz bio-signal frequencies. Separate power and ground planes are used in the PCB with analog and digital supply/gnd pairs separated into different grids to minimize noise coupling.

The output spectrum of the SAR ADC for a normalized full-scale input is plotted in Fig. 14(a); the measured SNR is  $\sim 44 \text{ dB}$  and SNDR is 40.6 dB (6.5-bit ENOB) for a 200 Hz BW which is suitable for ambulatory bio-signals. The measured DNL and INL values are shown in Fig. 14(b). The measured accuracy is less than the target 8-bit ENOB because of unavoidable parasitics in the C-2C array leading to static non-linearities and reduced full-scale range. On-chip calibration was not used.

The bandwidths of about 200 Hz and 1 kHz are adequate for most ambulatory and diagnostic bio-signals, respectively (Table I). At  $f_S = 2 \text{ kHz}$ , CS-AFE dissipates  $1.8 \mu\text{W}$  with  $M = 64$  active channels and  $28 \text{ nW}$  with  $M = 1$ . Because of the use of dual-gate devices and transistor stacking techniques the leakage power is limited to  $< 5\%$  of the total power dissipation.

Measured results of CS-AFE for a two-tone sinusoid are shown in Fig. 15 where  $CF$  ranges from 4 to 20. The signal is reconstructed using a Fourier basis for  $[\Psi]$  and CVX  $l_1$ -norm convex optimization [30].

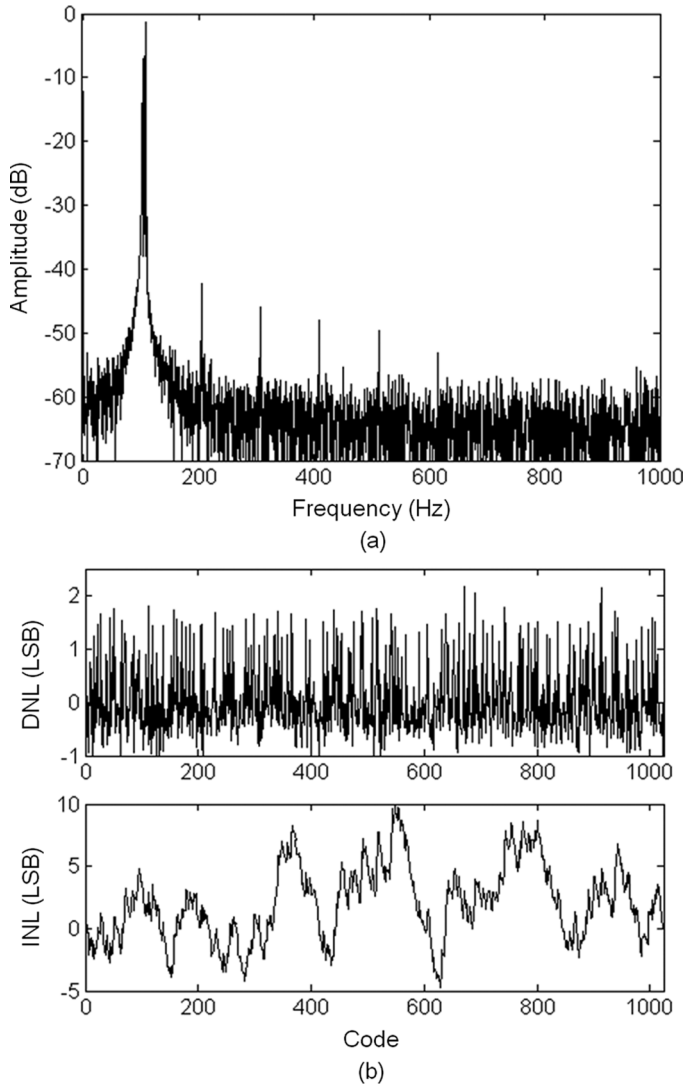


Fig. 14. SAR ADC performance. (a) Output spectrum normalized to full-scale; (b) DNL and INL.

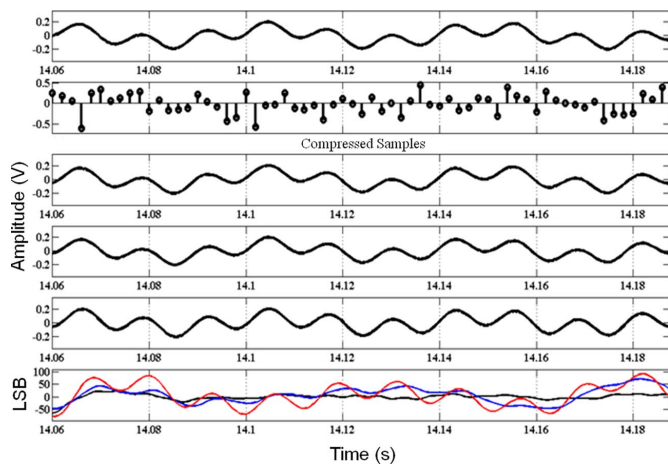


Fig. 15. Measured reconstructions for a two-tone signal (28 Hz and 50 Hz sinusoids). From the top: raw signal; stem plot of CS-AFE outputs for  $CF = 2$ ; reconstructed waveforms for  $CF = 4, 8$  and  $20$  with  $N = 256$  and  $M = 64, 32$  and  $13$ , respectively, and reconstruction error signals [black ( $CF = 4$ ), blue ( $CF = 8$ ) and red ( $CF = 20$ )] in LSBs where  $1 \text{ LSB} = 0.78 \text{ mV}$ .

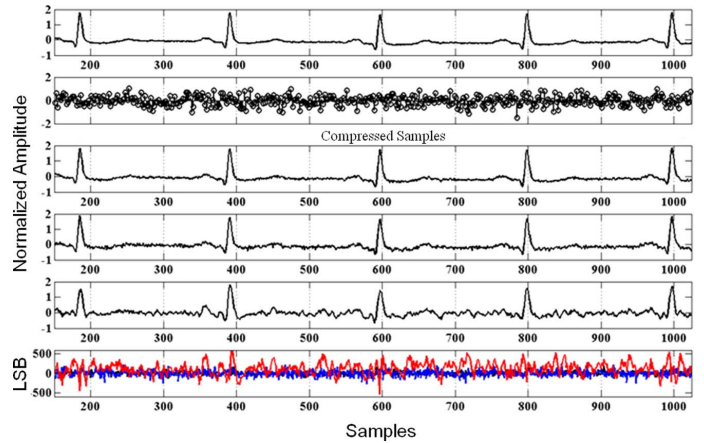


Fig. 16. Measured reconstructions of a synthesized ECG signal sparse in the Daubechies-4 wavelet domain using eight frames with  $N = 128$  samples each. From the top: raw ECG; stem plot of CS-AFE outputs; reconstructed waveforms with  $CF = 2, 4$ , and  $6$ , respectively, and reconstruction error signals [black ( $CF = 2$ ), blue ( $CF = 4$ ) and red ( $CF = 6$ )] in LSBs where  $1 \text{ LSB} = 0.78 \text{ mV}$ .

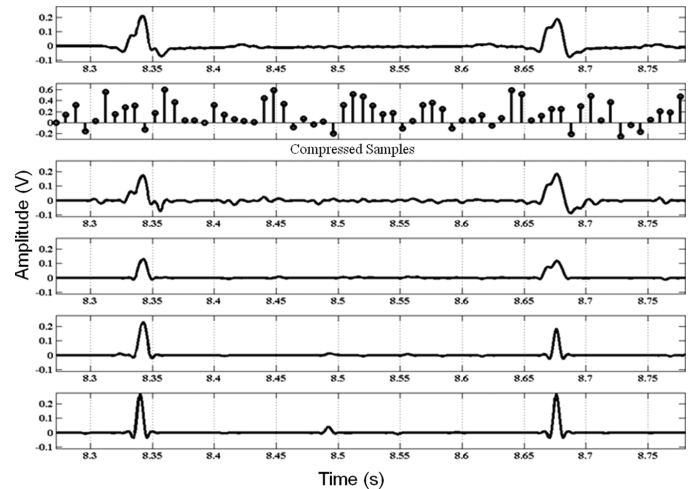


Fig. 17. Measured reconstructions of an ECG signal from the PhysioBank® database [19]: From top: raw ECG; stem plot of the CS-AFE outputs for  $CF = 2$ ; reconstructed ECG waveforms with  $CF = 2$  (non-thresholded),  $4, 8$  and  $16$  (thresholded) using  $N = 128$  and  $M = 64, 32, 16$ , and  $8$ , respectively.

Fig. 16 shows an un-thresholded ECG signal compressed by CS-AFE and reconstructed using a wavelet basis for  $[\Psi]$  derived from the Daubechies db4 mother-wavelet [31] using the Tree Matching Pursuit algorithm [12]. As expected, details of the ECG signal are reconstructed with  $CF = 4$ , but losses are observed at  $CF = 6$  and beyond because the sparsity of the ambulatory ECG signal is only about 95%.

Fig. 17 shows an example of CS compression and recovery where the ECG signal is first thresholded in the time-domain. Thresholding increases sparsity and enables an aggressive tradeoff between the compression factor and the level of detail. The raw ECG signal is compressed with  $CF = 2$  (not thresholded) and  $CF = 4, 8$ , and  $16$  (thresholded) and recovered in the time domain. Although many details are lost as  $CF$  increases, the locations and amplitudes of the  $QRS$  complexes are reasonably well preserved. Thus, for certain ambulatory applications, the  $R-R$  interval (i.e., the heart rate)

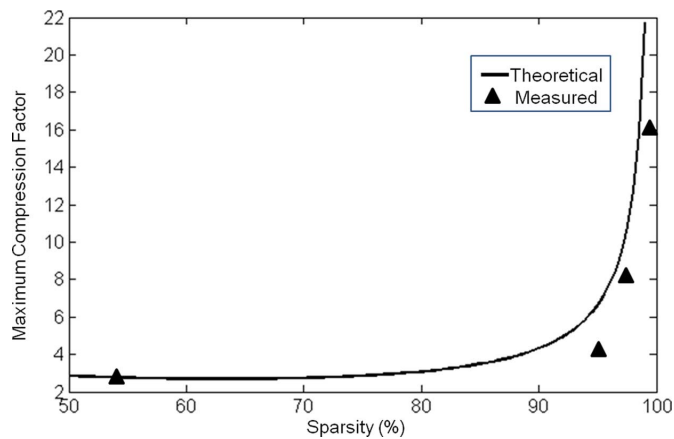


Fig. 18. Theoretical and measured  $CF$  vs. sparsity for time-domain-sparse ECG signals. Measured performance is reduced due to the non-ideal coherence and implementation losses.

TABLE III  
PERFORMANCE SUMMARY OF THE CS-AFE

Parameter	Value	
Technology	0.13 $\mu\text{m}$ CMOS	
Supply (V)	0.9 – 1.2	
Rows ( $M$ )	64	
Max. Input Sig. BW	1 kHz	
Measurement Matrix	Bernoulli and Uniform Random	
SAR ADC ENOB	6.5 bits	
DNL/INL (LSB)	2.2/10 @ 10-bit resolution	
Area	2 x 3 mm <sup>2</sup>	
Compression Factor	Two-tone Sinusoid (Fourier domain)	$CF = 1 - 20$
	ECG Signal (Wavelet domain)	$CF = 1 - 6$
	ECG Signal with thresholding (Time domain)	$CF = 1 - 16$
Power Consumption	1.8 $\mu\text{W}$ (64 CS Channels) [Static: 1.6 $\mu\text{W}$ , Dynamic 0.2 $\mu\text{W}$ ]	

is accurately recovered using CS-AFE in a high-compression ultra-low-power mode. Fig. 18 shows good agreement between the theoretical and measured  $CF$  vs. sparsity for time-domain-sparse ECG signals. The overall performance of CS-AFE is summarized in Table III.

## V. CONCLUSIONS

Wearable and wireless bio-sensors demand ultra-low power signal acquisition and transmission. Consequently, the data should be compressed at the sensor to enable efficient transmission to the data aggregator. The first fully-integrated compressed sensing analog-domain front-end, CS-AFE, for universal bio-signal sensing is demonstrated. It uses a pipelined column-wise multiplication scheme to achieve  $O(M)$  hardware complexity. An on-chip low-power area-efficient hybrid linear feedback shift register, HLFSSR, generates a pseudo-random 1-bit measurement matrix with similar performance to ideal Bernoulli matrices. Switched-capacitor C-2C MDAC/integrator and C-2C SAR ADC modules are designed using sub-threshold analog circuits and low-leakage switches. Theory, system design, circuit implementations and measurement results are presented. For ambulatory bio-sensor applications, CS-AFE enables a trade-off between feature accuracy and power con-

sumption using both wavelet- and time-domain reconstruction techniques. In normal usage where critical health events are rare, the need to operate in the low compression/high power mode occurs infrequently. Thus, CS-AFE achieves a universal bio-signal front-end with energy savings through sub-Nyquist operation of the data converters, elimination of the DSP circuitry and a significant reduction in the amount data to be transmitted.

## ACKNOWLEDGMENT

The authors thank Dr. J. A. Bolotski and Prof. S. Roy for useful discussions and A. Chen for layout assistance.

## REFERENCES

- [1] E. Jovanov, A. Milenkovic, C. Otto, and P. C. de Groen, "A wireless body area network of intelligent motion sensors for computer assisted physical rehabilitation," *J. NeuroEng. Rehabil.*, vol. 2, pp. 1–10, Mar. 2005.
- [2] R. F. Yazicioglu, P. Merken, R. Puers, and C. Van Hoof, "A 200  $\mu\text{W}$  eight-channel EEG acquisition ASIC for ambulatory EEG systems," *IEEE J. Solid-State Circuits*, vol. 43, pp. 3025–3038, Dec. 2008.
- [3] N. Verma, A. Shoeb, J. Bohorquez, J. Dawson, J. Guttag, and A. P. Chandrakasan, "A micro-power EEG acquisition SoC with integrated feature extraction processor for a chronic seizure detection system," *IEEE J. Solid-State Circuits*, vol. 45, pp. 804–816, Apr. 2010.
- [4] R. F. Yazicioglu, S. Kim, T. Torfs, H. Kim, and C. Van Hoof, "A 30  $\mu\text{W}$  analog signal processor ASIC for portable biopotential signal monitoring," *IEEE J. Solid-State Circuits*, vol. 46, pp. 209–223, Jan. 2011.
- [5] E. J. Candès, J. K. Romberg, and T. Tao, "Stable signal recovery from incomplete and inaccurate measurements," *Commun. Pure Appl. Math.*, vol. 59, pp. 1207–1223, Aug. 2006.
- [6] D. L. Donoho, "Compressed sensing," *IEEE Trans. Inform. Theory*, vol. 52, pp. 1289–1306, Apr. 2006.
- [7] D. L. Donoho, "For most large underdetermined systems of linear equations the minimal  $l_1$ -norm solution is also the sparsest solution," *Commun. Pure Appl. Math.*, vol. 59, pp. 797–829, Jun. 2006.
- [8] E. J. Candès and M. B. Wakin, "An introduction to compressive sampling," *IEEE Signal Process. Mag.*, vol. 25, pp. 21–30, Mar. 2008.
- [9] J. Romberg and M. B. Wakin, "Compressed sensing: A tutorial," in *Proc. IEEE Statistical Signal Processing Workshop*, Aug. 2007.
- [10] D. Needell and J. A. Tropp, "CoSaMP: Iterative signal recovery from incomplete and inaccurate samples," *Appl. Computat. Harmon. Anal.*, vol. 26, pp. 301–321, May 2008.
- [11] R. G. Baraniuk, V. Cevher, M. F. Duarte, and C. Hegde, "Model-based compressive sensing," *IEEE Trans. Inform. Theory*, vol. 56, pp. 1982–2001, Apr. 2010.
- [12] M. F. Duarte, M. B. Wakin, and R. G. Baraniuk, "Fast reconstruction of piecewise smooth signals from incoherent projections," in *Proc. Signal Processing with Adaptive Sparse Structured Representations Workshop*, Nov. 2005, pp. 1–4.
- [13] A. M. R. Dixon, E. G. Allstot, D. Gangopadhyay, and D. J. Allstot, "Compressed sensing system considerations for ECG and EMG wireless biosensors," *IEEE Trans. Biomed. Circuits Syst.*, vol. 6, pp. 156–166, Apr. 2012.
- [14] S. Mallat, *A Wavelet Tour of Signal Processing: The Sparse Way*. Boston, MA, USA: Elsevier Press, 2009.
- [15] E. G. Allstot, A. Y. Chen, A. M. R. Dixon, D. Gangopadhyay, and D. J. Allstot, "Compressive sampling of ECG bio-signals: Quantization noise and sparsity considerations," in *Proc. IEEE Biomedical Circuits and System Conf.*, Nov. 2010, pp. 41–44.
- [16] A. Salman, E. G. Allstot, A. Y. Chen, A. M. R. Dixon, D. Gangopadhyay, and D. J. Allstot, "Compressive sampling of EMG bio-signals," in *Proc. IEEE Int. Symp. Circuits and Systems*, May 2011, pp. 2095–2098.
- [17] Z. Lu, D. Y. Kim, and W. A. Pearlman, "Wavelet compression of ECG signals by the set partitioning in hierarchical trees algorithm," *IEEE Trans. Biomed. Eng.*, vol. 47, pp. 849–856, Jul. 2000.
- [18] H. Mamaghanian, N. Khaled, D. Atienza, and P. Vanderghyest, "Compressed sensing for real-time energy-efficient ECG compression on wireless body sensor nodes," *IEEE Trans. Biomed. Eng.*, vol. 58, pp. 2456–2466, Sep. 2011.
- [19] A. L. Goldberger, L. A. N. Amaral, L. Glass, J. M. Hausdorff, P. C. Ivanov, R. G. Mark, J. E. Mietus, G. B. Moody, C. K. Peng, and H. E. Stanley, "PhysioBank, PhysioToolkit, and PhysioNet: Components of a new research resource for complex physiologic signals," *Circulation*, vol. 101, pp. 215–220, Jun. 2000.

- [20] S. Kirolos, J. N. Laska, M. Wakin, M. Duarte, D. Baron, T. Ragheb, Y. Massoud, and R. Baraniuk, "Analog-to-information conversion via random demodulation," in *Proc. IEEE Dallas/CAS Workshop on Design, Applications, Integration and Software*, 2006, pp. 71–74.
- [21] T. Ragheb, J. N. Laska, H. Nejati, S. Kirolos, R. G. Baraniuk, and Y. Massoud, "A prototype hardware for random demodulation based compressive analog-to-digital conversion," in *Proc. IEEE Midwest Symp. Circuits and Systems*, Aug. 2008, pp. 37–40.
- [22] M. Mishali, Y. C. Eldar, and A. J. Elron, "Xampling: Signal acquisition and processing in union of subspaces," *IEEE Trans. Signal Process.*, vol. 59, pp. 4719–4734, Oct. 2011.
- [23] J. Yoo, S. Becker, M. Loh, M. Monge, E. Candès, and A. Emami-Neyestanak, "A 100 MHz–2 GHz  $12.5 \times$  sub-Nyquist-rate receiver in 90 nm CMOS," in *IEEE Radio Frequency Integrated Circuits Symp. Dig.*, 2012, pp. 31–34.
- [24] F. Chen, A. P. Chandrakasan, and V. M. Stojanović, "A signal-agnostic compressed sensing acquisition system for wireless and implantable sensors," in *Proc. IEEE Custom Integrated Circuits Conf.*, 2010, pp. 1–4.
- [25] F. Chen, A. P. Chandrakasan, and V. M. Stojanović, "Design and analysis of a hardware-efficient compressed sensing architecture for data compression in wireless sensors," *IEEE J. Solid-State Circuits*, vol. 47, pp. 744–756, Mar. 2012.
- [26] E. G. Allstot, A. Y. Chen, A. M. R. Dixon, D. Gangopadhyay, H. Mitsuuda, and D. J. Allstot, "Compressed sensing of ECG bio-signals using one-bit measurement matrices," in *Proc. IEEE Int. NEWCAS Conf.*, 2011, pp. 213–216.
- [27] N. Verma and A. P. Chandrakasan, "An ultra low energy 12-bit rate-resolution scalable SAR ADC for wireless sensor nodes," *IEEE J. Solid-State Circuits*, vol. 42, pp. 1196–1205, Jun. 2007.
- [28] E. Alpman, H. Lakdawala, L. R. Carley, and K. Soumyanath, "A 1.1 V 50 mW 2.5 GS/s 7 b time-interleaved C-2C SAR ADC in 45 nm LP digital CMOS," in *IEEE Int. Solid-State Circuits Conf. Dig.*, 2009, pp. 76–77.
- [29] D. J. Allstot, "A precision variable-supply CMOS comparator," *IEEE J. Solid-State Circuits*, vol. 17, pp. 1080–1087, Dec. 1982.
- [30] M. C. Grant, S. P. Boyd, and Y. Ye, CVX: MATLAB Software for Disciplined Convex Programming, 2013 [Online]. Available: <http://cvxr.com/cvx>, 2.0
- [31] I. Daubechies, *Ten Lectures on Wavelets*. Philadelphia, PA, USA: SIAM, 1992.



**Daibashish Gangopadhyay** (S'06–M'12) received the B.Tech. and M.Tech. degrees in electronics and electrical communication engineering from the Indian Institute of Technology, Kharagpur, India, in 2005 and 2006, respectively, and the Ph. D. degree in electrical engineering from the University of Washington, Seattle, WA, USA, in 2011.

During 2008–2009 he was with Qualcomm, San Diego, where he worked on bio-sensor circuits for personal area network applications. Since 2012 he has been with Marvell Semiconductor, Santa Clara,

CA, USA, focusing on RF and analog-mixed ICs for connectivity and cellular applications. His research areas are wireless RF/mixed-signal integrated circuits and systems, bio-signal sensors and signal processing.

Dr. Gangopadhyay received the IEEE RFIC Symposium Best Student Paper Award in 2011, the Analog Devices Outstanding Student Designer Award in 2010 and Indian National Academy of Engineering's Innovative Projects Award in 2006.



**Emily G. Allstot** (S'10) received the B.S. degree in electrical engineering from the University of Washington (UW), Seattle, WA, USA, where she is currently pursuing the M.S.E.E. degree.

Her research interests include analog circuits and systems, biomedical instrumentation, and compressed sensing.

She was awarded an Undergraduate Research Opportunities (URO) Scholarship from the Semiconductor Research Corporation in 2011–2012. She served as the Public Relations officer for the UW

IEEE Student Branch and as a summer intern for the Signal and Datapath Solutions (SDS) group at Texas Instruments, Inc., Santa Clara, CA, USA, in 2012.



**Anna M. R. Dixon** received the B.S. degree and the M.S. degree from The Ohio State University, Columbus, OH, USA, in 2006 and 2008, respectively, and the Ph.D. degree from the University of Washington, Seattle, WA, USA, in 2012.

Her research interests include low-power biomedical instrumentation, circuits and systems design, and compressed sensing.

Dr. Dixon was awarded an Intel/SRCEA Master's Scholarship for 2006–2008 and the Intel/SRCEA Graduate Fellowship for 2011–2012. She received the Analog Devices Inc. Outstanding Student Analog Designer Award in 2011.



**Karthik Natarajan** (S'06–M'12) received the Bachelor degree from BMS College of Engineering, Bangalore, India, in 2004. He received the M.S. and Ph.D. degrees from the University of Washington, Seattle, WA, USA, in 2008 and 2012, respectively.

He has held RF/Analog circuit design internship positions in Cypress Semiconductors and Intel Corporation. Prior to starting his graduate study at University of Washington, Seattle, he worked on custom digital integrated circuit design in LSI Logic, Bangalore. He is currently with the Wireless Research

group at Intel Corporation, Hillsboro, OR, USA. His research interests include low-power analog and RF communication circuits.



**Subhanshu Gupta** (S'03–M'11) received the B.E. degree from the National Institute of Technology, Trichy, India, in 2002, and the M.S. and Ph.D. degrees from the University of Washington, Seattle, WA, USA, in 2006 and 2010, respectively.

He interned with National Semiconductor (now Texas Instruments), Santa Clara, CA, USA, from 2005 to 2006, where he worked on high-resolution sigma-delta ADCs. Since 2011, he has been with RFIC/Mixed Signal group at Maxlinear Inc., Irvine, CA, USA, working on wideband ADCs

and DACs for satellite/cable TV applications. His current research interests include architectures for direct-RF wideband sampling ADCs and wideband transmitter DACs, millimeter-wave architectures for backhaul data centers and applications of CMOS digital signal processing solutions for biological and environmental sensors.

Dr. Gupta received the Analog Devices Outstanding Student Designer Award in 2008 and an IEEE RFIC Symposium Best Student Paper Award in 2011.



**David J. Allstot** (S'72–M'72–SM'83–F'92–LF'12) received the B.S., M.S., and Ph.D. degrees from the University of Portland, Oregon State University, and the University of California, Berkeley, respectively.

He has held several industrial and academic positions. Most recently, he was the Boeing-Egvedt Chair Professor of Engineering at the University of Washington from 1999 to 2012 and Chair of the Department of Electrical Engineering from 2004 to 2007. In 2012 he was a Visiting Professor of Electrical Engineering at Stanford University and since

2013 he is the MacKay Professor in Residence in the EECS Department and Executive Director of the Berkeley Wireless Research Center at UC Berkeley.

Dr. Allstot has advised approximately 60 M.S. and 40 Ph.D. graduates, published more than 300 papers, and received several awards for outstanding teaching and graduate advising as well as research awards including the 1980 IEEE W.R.G. Baker Award, 1995 and 2010 IEEE Circuits and Systems Society (CASS) Darlington Award, 1998 IEEE International Solid-State Circuits Conference (ISSCC) Beatrice Winner Award, 1999 IEEE CASS Golden Jubilee Medal, 2004 IEEE CASS Charles A. Desoer Technical Achievement Award, 2005 Semiconductor Research Corp. Aristotle Award, 2008 Semiconductor Industries Assoc. University Research Award, and 2011 IEEE CASS Mac Van Valkenburg Award. He has been active in service to the IEEE Circuits and Systems and Solid-State Circuits Societies throughout his career.